Petroleum and Coal

Article **Open Access**

Numerical Modeling of Water-Oil Two-Phase Flow During Counter-Current Spontaneous Imbibition in Porous Media at Pore-Scale

*Iman Jafari[1] and Amir H. Mohammadi[2]**

[1] *Department of Chemical Engineering, Jask Branch, Islamic Azad University, Jask, Iran*
[2] *Discipline of Chemical Engineering, School of Engineering, University of KwaZulu-Natal, Howard College Campus, King George V Avenue, Durban 4041, South Africa*

Received April 24, 2021; Accepted October 8, 2021

Abstract

In the current work, a phase-field method has been used to develop a numerical model in order to simulate two-phase flow of water and oil through a heterogeneous fractured porous medium. An accurate finite element solver based on Comsol Multiphysics was applied to solve the Cahn–Hilliard phase-field method coupled with Navier–Stokes and continuity equations. A two-dimensional (2D) heterogeneous matrix block and an adjacent fracture were constructed for considering the computational domain. To deal with a more realistic reservoir settings, both matrix block and the fracture were initially oil saturated and then water injection was applied to maintain continuous water supply and also expel the oil phase. Various sensitivity analyses were performed to assess the impacts of wettability, fracture aperture, interfacial tension, and water injection velocity on the process of displacement. It was observed that the water mass imbibed into the matrix block varies linearly with time before the water front meets the outlet, known as "filling fracture" regime, which is captured for the first time in a numerical study. Increasing interfacial tension increases imbibition rate and ultimate oil recovery. Variation of the position of interface/ wall contact point with time for model of 50 mN/m IFT indicates contact angle alteration during the imbibition process. Increasing the fracture aperture reduces water breakthrough time and oil recovery; but it has a negligible effect on ultimate recovery. The results indicate that the model with the highest injection velocity of 5 mm/s recovered the matrix oil by 14% in the first 5 s and rapidly reached its ultimate recovery. However, for the lowest injection velocity of 0.05 mm/s the lowest imbibition rate and highest ultimate recovery of 65% were observed. It is revealed that at higher injection velocities, the water infiltration path is less selective compared to the other cases; consequently, the water front progresses almost uniformly downward, known as, "instantly filled fracture" regime. The developed model has captured three pore-level mechanisms, including fluids' reverse displacement, water bridging, and interface coalescence successfully.

Keywords: *Counter-current spontaneous imbibition; Wettability; Fracture aperture; Interfacial tension; Water injection velocity.*

1. Introduction

Flowing of fluids especially with two phases in subsurface porous and permeable media has received significant attention since the last decades due to its application in various fields including hydrocarbon recovery, sequestration of carbon dioxide, and waste disposal [1-8]. Therefore, it has been of great interest to investigate the influences of different factors such as heterogeneity, capillarity, wettability and viscosity, on this process to reduce the flow instabilities which cause inefficient immiscible displacements [9]. Other key parameters affecting the process are rock fractures and their geometrical characteristics [10]. The interaction between three forces of gravity, capillary and viscous, determine pore-scale process and macroscopic configuration of the multiphase flow [11]

In the petroleum context, the process of wetting phase displacement using non-wetting phase is referred as drainage, and the imbibition process is the non-wetting phase displace-

ment by the wetting phase [12]. Spontaneous imbibition (SI) refers to a process that the capillary forces suck the wetting phase into porous media , and the non-wetting phase is expelled into the fracture [13]. A fundamental mechanism in water-wet fractured reservoirs for recovery of oil is SI of water into the oil-saturated matrix blocks [14-15]. The process of SI can be classified into co-current or counter-current SI. Co-current SI occurs when two-phase flow of oil and water is in the same direction. While, in the counter-current SI, fluids flow in the opposite directions [16-17].

During the past decades, a large number of core-scale experiments have been implemented to understand the influences of various mechanisms on the interactions between matrix and fracture (See Morrow and Mason [18] and Mason and Morrow [19]). Rangel-German and Kovscek [20] used X-ray computerized tomography (CT) images to study the capillary imbibition in fractured mediums. Based on different values of the fracture aperture and injection rate, two different regimes of flow in fracture were observed. The regime of "Filling fracture" is identified during relatively slow advancement of water inside the fracture which can be characterized by a 2D imbibition pattern. While, in the regime of "Instantly filled fracture", the required time to fill the fracture is much less than the time needed for imbibition. In this regime, a 1D water advancement was observed. Fernø *et al.* [21] used magnetic resonance imaging (MRI) to study the fluid displacements by conducting oil- and water-flooding experiments. The mechanism of reoccurring droplet growth-detachment-growth was captured. It was determined that in an open fracture, the water bridges development consists of three regimes including bridge-growth, fracture-filling, and fracture-filled.

The physical and micro-constructed models of the porous media (micromodels) have been extensively applied to visualize the relevant factors influences on the fluids flow in porous media [22-24]. However, few studies have focused to investigate the multiphase flow in fractured porous media using micromodels [25]. Rangel-German and Kovscek studied water infiltration in fractured porous media using an etched-silicon-wafer micromodel [26]. It was indicated that during the imbibition, while oil blobs detached from the surface, they grew into the fracture. It was also demonstrated that the size of the growing oil droplets on the fracture is affected by fluid flow rate. Using silicon-etched micromodel, Hatiboglu and Babadagli [27] showed that the structure and size of pore and throat determine the residual oil development.

Laboratory experiments are costly and time-consuming [28]. Thus, several detailed simulation techniques, which simulate multiphase flow in complex porous structures, have been developed [29-30]. Among them, pore network modeling [31-32], lattice Boltzmann [33-34], level set [25-36], phase-field [37-41], and volume of fluids based finite volume [42-43] have been the most popular methods. For the first time, Hatiboglu and Babadagli [27] developed a pore-scale lattice Boltzmann model to describe the SI into oil-saturated porous media. Residual oil saturation development was captured and it was found that water recovery is directly related to the pore structure and changing the wettability did not affect the ultimate recoveries. They also showed a limitation of using lattice Boltzmann method for two-phase flow of water and oil at high viscosity ratios above four. Gunde *et al.* [44] applied the two-color lattice Boltzmann method to predict the two-phase relative permeabilities during capillary driven counter-current flow through a fractured media for oil-water system. They investigated the development of kerosene-water interface at the scale of pore. They showed that the values of oil phase relative permeability are approximately half of the co-current case corresponding values. It was observed that water capillary imbibition and kerosene simultaneous expulsion take place in smaller pores and relatively larger pores, respectively. The relative permeability of oil increases by interfacial tension (IFT) reduction. Andersen *et al.* [45] proposed a simple one dimensional model for SI to study the influences of different parameters such as different viscosity relations, injection rate, and saturation functions. In addition, the constructed model was able to capture the two "filling fracture" and "instantly filled" regimes which were reported and discussed in Rangel-German and Kovscek work [20].

Akhlaghi Amiri and Hamouda compared level-set and phase-field techniques using various criteria such as accuracy, running time, and pore-scale events capturing capability. They found that the phase-field method is superior over level set for complex porous medium [46]. Using

Comsol Multiphysics, Akhlaghi Amiri and Hamouda [9] studied the problem of flow instabilities during displacement for uniform and dual permeability media. It was shown that as the medium gets more water-wet, the water film becomes thicker. In addition, as the porous medium becomes less water-wet, the wetting phase disintegrates into several thin water fingers with a mean thickness of less than pore body. Their results also revealed that the water saturation increases by capillary number for different mobility ratio values during water-oil displacement. Maaref *el al.* [11] used the phase-field method to study the influences of wettability, heterogeneity, and viscosity ratio on the displacement of water-oil system in micromodel media. The obtained results showed that when the medium becomes more heterogeneous, the oil recovery factor decreases as a result of oil phase trapping. Two mechanisms of water blob trapping and water finger splitting in the pore-scale were observed for neutral and oil-wet mediums. Rokhforouz and Akhlaghi Amiri [17] performed a simulation study to investigate the countercurrent spontaneous imbibition in a fractured porous media, where the fracture and matrix blocks were first saturated with oil and water, respectively. The influences of wettability, interfacial tension, and viscosity ratio during the countercurrent imbibition process were assessed. Jafari *et al.* [39] used the same method to study the effects of fracture aperture, water injection velocity, and grain shape during countercurrent spontaneous imbibition. Using a lattice Boltzmann (LB) color-gradient model, Gu *et al.* [48] studied the effects of water injection velocity, geometry configuration of the dual permeability zones, interfacial tension, viscosity ratio, and fracture spacing in a synthetic porous media constructed by a Voronoi tessellation technique. Initial presence of oil phase in the fracture is often the only possible situation occurs in the fractured reservoirs. This manuscript deals with a more realistic situation where both matrix and fracture are initially saturated with oil and then water invasion occurs, which differentiate it from previous works. It can be expected that fluid interactions are different from the situation where the porous matrix is initially fully saturated with the oil phase, while the fracture is initially saturated with the water phase. In the current study, the method of phase-field was applied to investigate the effects of wettability, fracture aperture, water-oil IFT, and water injection velocity on the displacement process. The results give an insight into better understanding of the underlying physics of the counter-current spontaneous imbibition in fractured porous and permeable media.

2. Numerical model

In the current study, 2D rectangular heterogeneous porous medium with fracture is considered to simulate a matrix block. The dimension of the rectangle is with respectively porosity and permeability of 35% and 8.9 e^{-10} m^2. The grains distribution is represented using an equilateral triangular array of circles with various diameters. To create heterogeneity, grain diameters in the range of 0.6 up to 1.15mm were used. The fracture is represented using a rectangle with the dimension of located close to the porous matrix. Permeability of the fracture is about 2.5 e^{-8} m^2. The average pore and throat diameter are set to 1.3 e^{-3} and 2.2 e^{-4} m, respectively. Figure 1 illustrates constructed domain for the numerical experiments.

Water is injected to the model from the fracture itself. The 2D model is discretized using predefined "normal" mesh density with triangular elements as a specific refinement level of the physics-controlled meshing methods built into the computational software. Figure 2 depicts a magnified view of the discretized system. Considering coarser mesh grids in the bulk and denser mesh grids covering the boundary layers will reduce computational time and will result in better convergence [49]. Grid sensitivity study indicates that the water and oil saturations have no significant relation with number of grid elements (Figure 3). Therefore, the "normal" mesh density is applied during all numerical experiments. The recovery factor is defined as the ratio of the total recovered oil to the total reservoir oil. In addition, the dimensionless time is defined as $t_D=t/t_{breakthrough}$.

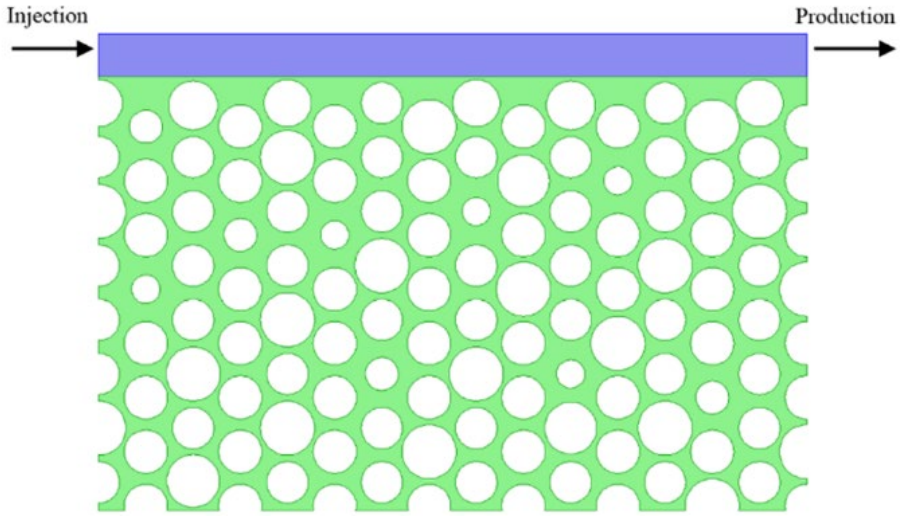

Figure 1. Schematic representation of constructed fractured heterogeneous porous media. The green and blue areas represent the matrix block and fracture, respectively

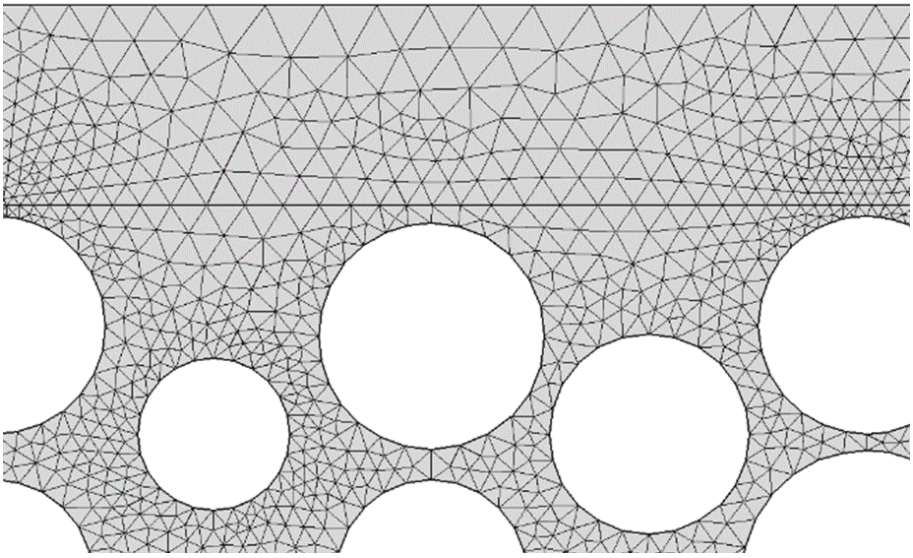

Figure 2. Mesh generation for the simulated domain. Note how meshes are refined at the boundaries

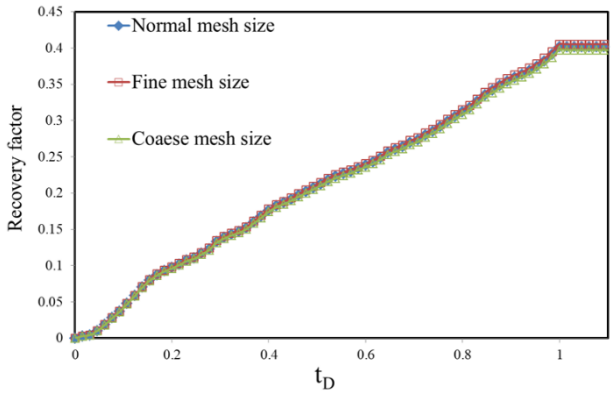

Figure 3. Matrix oil recovery factor versus dimensionless time for three mesh sizes

To solve the interfacial problems of the counter-current SI, the phase-field equation is coupled with the continuity and modified Navier-Stokes equations. The modified Navier-Stokes equations represent momentum conservation, and continuity represents mass conservation for flowing fluids at porous media. Cahn–Hilliard phase-field technique is implemented to identify a diffusive interface separating the immiscible phases. The fourth order partial differential equation of Cahn-Hilliard [50] is decomposed into two second order partial differential equation through applying an auxiliary parameter (Ψ) [51]. It is assumed that each phase is incompressible and the phase change does not occur. In addition, gravity forces are ignored by considering 2D horizontal flow. The system of equations is as below:

$$\nabla . \boldsymbol{u} = 0 \quad (1)$$

$$\rho \frac{\partial \boldsymbol{u}}{\partial t} + \rho(\boldsymbol{u} \cdot \nabla)\boldsymbol{u} = -\nabla p + \nabla \cdot [\mu(\nabla u + \nabla u^T)] + G\nabla\varphi \quad (2)$$

$$\frac{\partial \varphi}{\partial t} + \boldsymbol{u} \cdot \nabla\varphi = \nabla \cdot (\frac{\gamma\lambda}{\varepsilon^2})\nabla\psi \quad (3)$$

$$\psi = -\nabla\varepsilon^2\nabla\phi + (\phi^2 - 1)\phi \quad (4)$$

where u denotes fluid flow velocity; p represents pressure; t is time; ρ is weighted average of the fluid components density; μ is weighted average of the fluid components dynamic viscosity; ϕ represents phase-field order parameter and G is the chemical potential. In addition, Ψ is the auxiliary parameter; ε is capillary width; γ is mobility; and λ is the mixing energy density.

The region with the dimensionless phase-field parameter (ϕ) between -1 and 1 is defined as the diffusive interface. The relative concentrations of the two components are $\frac{1+\phi}{2}$ and $\frac{1-\phi}{2}$based on phase-field parameter. In this notion, the two phases are represented by $\phi = \pm 1$ and the interface is represented by. Using , the physical properties of diffusive interface are as follow:

$$\upsilon(\phi) = \frac{1+\phi}{2}\upsilon_o + \frac{1-\phi}{2}\upsilon_w \quad (5)$$

where υ represents individual phase property like density (ρ) and viscosity (μ). Further information about the phase-field theory is available in literature [52-55].

The porous matrix and fracture are oil phase saturated initially. Water with a constant velocity of (u_{inj}= 0.0005 m/s) is injected at the inlet of the fracture to maintain continuous water supply and expel the oil phase. The outlet has zero pressure. No-slip boundary conditions (u=0) are considered on the matrix block' edges for establishing a counter-current interaction of the model. The grain surfaces are considered as wetted walls with a specific contact angle. On the solid wetted grains, the following boundary conditions are imposed:

$$\boldsymbol{u} = 0 \quad (6)$$

$$n \cdot \varepsilon^2\nabla\varphi = \varepsilon^2 \cos(\theta)|\nabla\varphi| \quad (7)$$

$$n \cdot (\frac{\gamma\lambda}{\varepsilon^2})\Delta\psi = 0 \quad (8)$$

where n denotes unit normal to the wall, θ and is the contact angle. Densities of oil and water are respectively 800 and 1000 kg/m^3. Both fluids' viscosities are also considered equal to 0.001 Pa.s.

Comsol software was employed to solve the governing equations based on the finite element method. A predefined time dependent laminar two-phase flow located in the "Multiphase flow" module, was utilized [51]. The simulation time step was δt = 1 s. It should be noted that the governing equations were solved in 2D. The model and mesh convergence are satisfied for the phase-field method by considering the average grain diameter in the porous medium as the characteristic length (l_c) and defining Cahn number as $Cn=\varepsilon/l_c$ at Cn=0.03 and mesh size $h = 0.8\varepsilon$. The results of simulations with $\gamma_c = 1$ indicated less volume shrinkage and more physically realistic outcomes [46]. These values were employed in all numerical experiments.

3. Results and discussion

3.1. Impact of wettability on the fluid flow in porous media

In a system of multiphase fluids, the tendency of a rock surface to preferentially contact a particular fluid is referred to wettability [56]. The contact angle (θ) of liquid/vapor interface

with a solid surface is used to determine the degree of wettability [57]. Depended on the contact angle's value, the reservoir rock surface can be water-wet ($\theta < \frac{\pi}{2}$), oil-wet ($\theta > \frac{\pi}{2}$), or neutral-wet ($\theta = \frac{\pi}{2}$). Wettability of the porous media is an important factor, which affects the flow mechanisms and porous media properties at the levels of microscopic and macroscopic [58]. In this part, models with various contact angles were simulated to understand the impact of wettability on two-phase flow in the porous media during the counter-current SI.

Figure 4 shows the water-oil distributions during the imbibition process in the extremely water-wet model $\left(\theta = \frac{\pi}{10}\right)$ for different times.

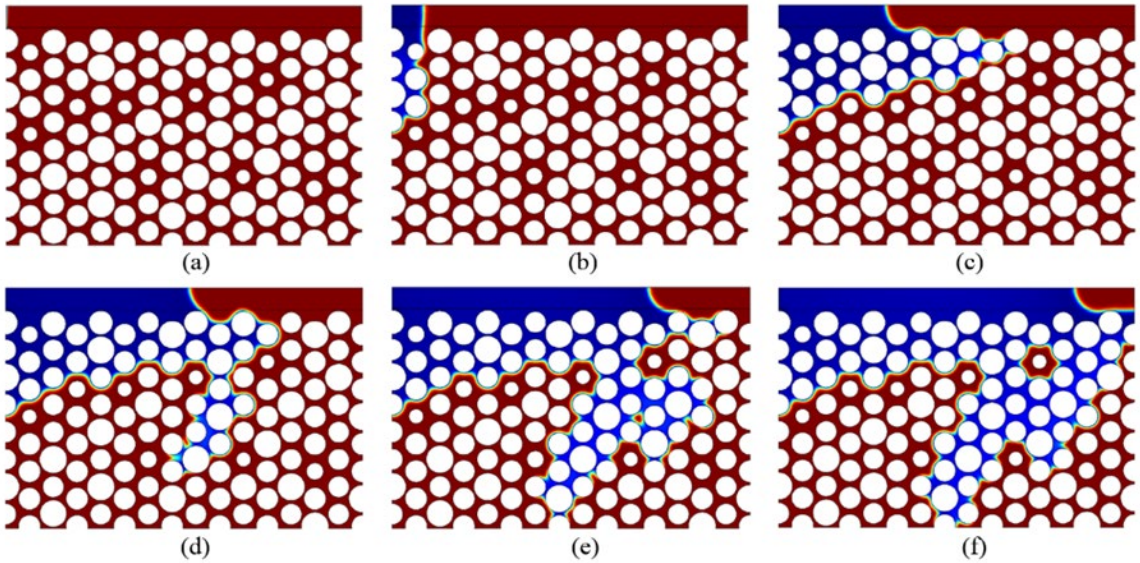

Figure 4. Fluid distributions at six different dimensionless times during counter-current SI for the simulated model with $\theta_c = \frac{\pi}{10}$ (a) t_D = 0, (b) t_D = 0.1, (c) t_D = 0.4, (d) t_D = 0.6, (e) t_D = 0.85, (f) t_D = 1

Firstly, the matrix and the adjacent fracture were saturated with oil, and then water was injected through the inlet (Figure 4a). The oil and water phases respectively are represented by red and blue colors, and the color gradient represents the interface mixing zone. Through water injection into the fracture, water was sucked into the porous medium with the sizes of 2-3 pore bodies and also progressed to the fracture (Figure 4b). It can be seen from Figure 4c that the matrix oil was displaced by water phase and the water front was narrowed from 4 pore bodies to a pore body. It is indicated that the wetting phase firstly fills the small size pores and throats, which is in accordance with micromodel observations conducted by Hatiboglu and Babadagli [27]. Water phase gradually floods the fracture and displaces the resident oil. Figure 4d shows that the water phase is progressed by forming a capillary finger with a mean width of 1-3 of pore bodies. This kind of instability occurs in the form of wide forward and lateral moving fronts of displacing phase with a mean width of more than 1-3 of pore bodies, that is in agreement with the experimental study of Lenormand *et al.* [59]. Afterwards, another capillary finger is formed in the medium right-hand side and the formed finger is thickened through occupying more pore bodies (Figure 4e). It can also be seen that small droplet of oil is trapped between three grains because of water bridging between adjacent grains. The imbibition process is stabilized after 65 s and 40% of matrix oil recovery (Figure 4f). In different zones of porous medium, water-oil interface stops progressing as it reaches wider pores and throats.

Figure 5 summarizes the results obtained for all models with various grain's contact angles, $\theta = \frac{\pi}{10}$ up to $\theta = \frac{\pi}{2}$, during the imbibition process. Recovery factor is referred to the ratio of matrix oil recovery to the total oil of matrix. As can be seen, the water mass imbibed into the matrix block varies linearly versus dimensionless time until the water front meets the outlet.

This curve is characterized by "filling fracture" regime which was identified by Rangel-German and Kovscek using X-ray CT scanning [20]. Alteration of wettability from neutral–wet to strongly water wet increases imbibition rate and ultimate recovery, which is in agreement with the previous experimental findings [60]. For example, ultimate oil recovery in neutral-wet medium (π/2) is about 11%, while it is more than 40% for the extremely water-wet medium$\left(\theta = \frac{\pi}{10}\right)$. It is also found that increasing the contact angle results in an earlier breakthrough time.

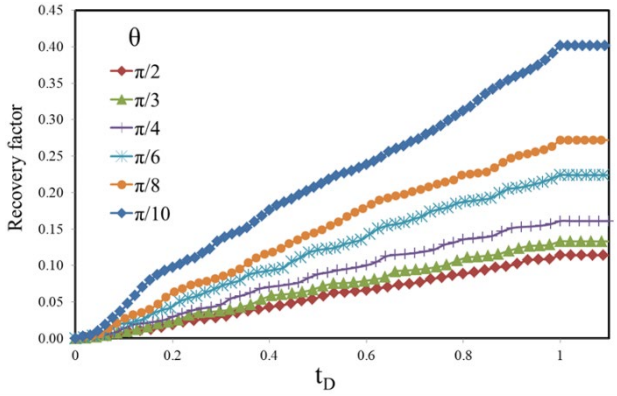

Figure 5. The matrix oil recovery factor as a function of dimensionless time for different models with contact angles of π/2, π/3, π/4, π/6, π/8 (the base case), and π/10

Figure 6 depicts the stabilized distribution of oil and water for models with various wettability states. According to the equation of Young–Laplace, $p_c = \frac{2\sigma \cos\theta}{r}$, where p_c represents capillary pressure and r is the capillary radius based on pore and throat sizes, for cases with neutral wet medium$(\theta = \frac{\pi}{2})$, the capillary pressure is zero and capillary fingers do not form. Thus, water imbibition and matrix oil expulsion do not occur. Water phase stops moving toward the porous matrix and no more production is observed (Figure 6a). The models with $\theta = \frac{\pi}{3}$ and $\frac{\pi}{4}$ show higher imbibition rate as a result of increased capillarity level and water invades the neighboring grains of the fracture (Figure 6b, c). Water imbibed zones become wider when θ decreases $(\theta < \frac{\pi}{4})$ and it forms a front with a regular shape and negligible fingers. The wetting phase front stops progressing as it reaches larger pores and throats (Figure 6d, e). In the extremely water-wet matrix $(\theta = \frac{\pi}{10})$, the capillary fingers formed by water phase propagate deeply into the matrix and one oil drop is trapped in the middle of matrix block (Figure 6f). These results are qualitatively similar to numerical results of Rokhforouz and Akhlaghi Amiri, where the fracture and matrix block were initially saturated with oil and then with water [47].

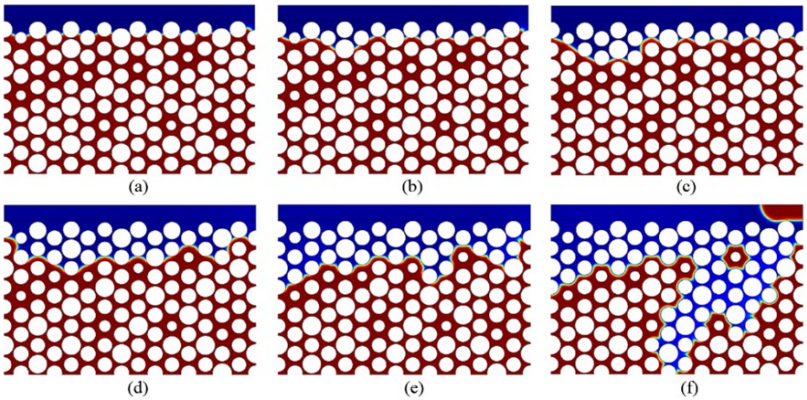

Figure 6. Snapshots of the stabilized fluid distributions for different models with contact angles of (a) π/2, (b) π/3, (c) π/4, (d) π/6, (e) π/8, and (f) π/10

3.2. Effect of fracture aperture on the fluid flow in the porous media

To understand the effect of fracture geometrical characteristic models three different fractures with 0.45, 0.90 (the base case), and 1.25 mm of apertures were simulated. Figure 7 shows the matrix oil recovery versus dimensionless time for imbibition process of the mentioned models. According to this figure, generally, by increasing the fracture aperture the imbibition rate will increase at early times. The model of widest fracture aperture reached to its ultimate recovery factor first, after 50 s. However, the model with the narrowest aperture continued imbibition process until 97s and its ultimate matrix oil recovery was about 0.3.

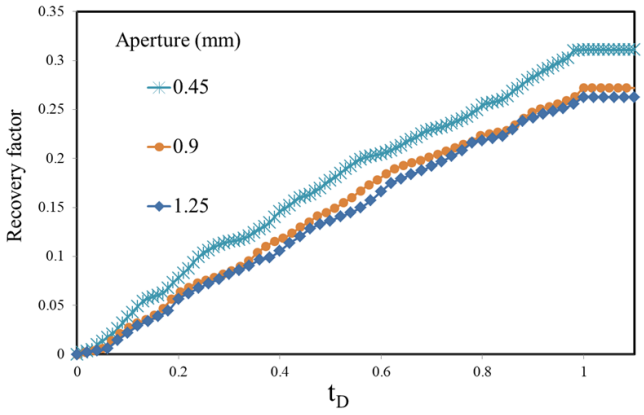

Figure 7. The matrix oil recovery factor as a function of dimensionless time for three models with fracture apertures of 0.45, 0.90 and 1.25 mm

Figure 8 illustrates the water and oil stabilized distributions for these models. For the case with the fracture aperture of 0.45 mm, more pore bodies in the medium left-hand side were invaded compared with the other models and consequently higher water saturation can be expected.

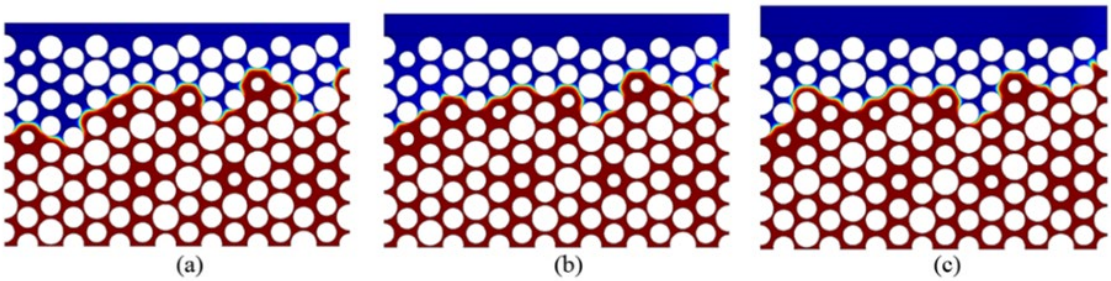

Figure 8. Snapshots of the stabilized fluid distributions for three models with different fracture apertures of (a) 0.45 (b) 0.90 and (c) 1.25 mm

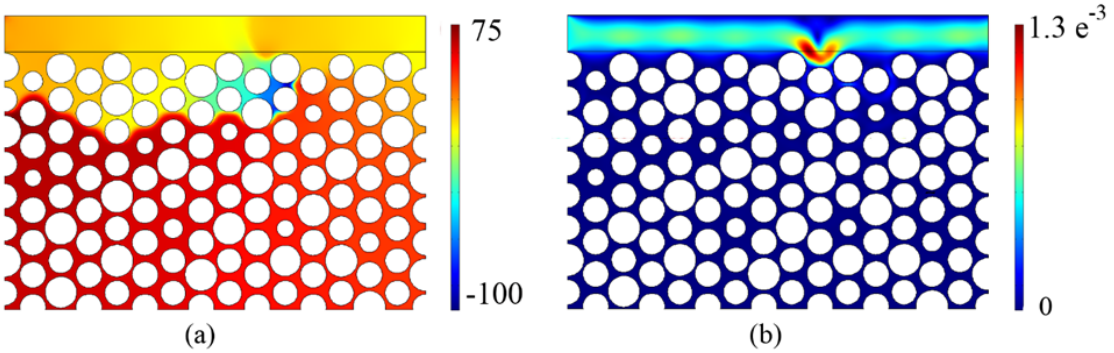

Figure 9. (a) velocity (m/s) and (b) Pressure (Pa) distribution profiles at t_D = 0.3 for the simulated model with fracture aperture of 1.25 mm

Figure 9 shows the velocity and pressure fields of the model for widest aperture at t_D = 0.3. A pressure gradient between the phases of advancing and receding in the matrix, i.e., capillary pressure (p_c), can be identified. To expel the oil from matrix into the fracture, it is observed that the pressure of the water front decreases to lower values in the middle of the medium. Figure 9b shows the main water and oil streamlines inside the fracture and matrix based on velocity profile.

3.3. Effect of IFT on the fluid flow in the porous media

This section investigates the effect of IFT on displacements of two-phase flow of water and oil in heterogeneous fractured porous media for the cases with the initially oil saturated matrix block and fracture. Figure 10 shows the matrix oil recovery versus dimensionless time for three models with IFTs of 5, 25 (the base case), and 50 mN/m. It can be observed that higher water-oil IFT causes higher imbibition rate and ultimate oil recovery. As an example, in the first 50 s, 16% of the matrix oil is recovered in the model with the lowest IFT, while for the models with the highest IFT, the ultimate oil recovery is above 30%. It is also revealed that increasing the IFT leads to a delayed breakthrough time. These results are in accordance with the Young–Laplace equation, which states increasing the IFT will cause higher capillary pressure, and consequently higher water imbibition rate. A stabilized distribution of water and oil for the cases with various IFTs is shown in Figure 11.

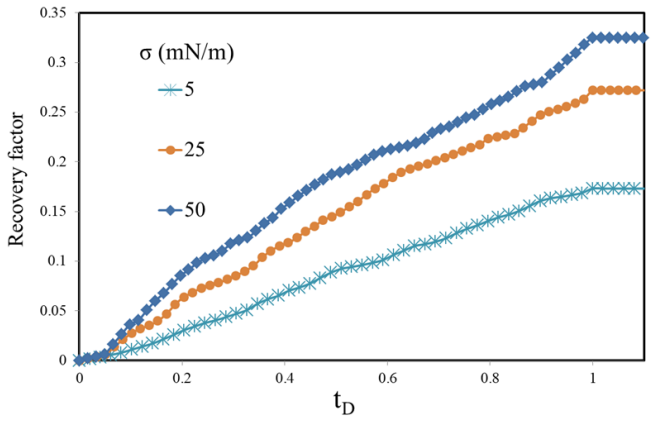

Figure 10. The matrix oil recovery factor as a function of dimensionless time for three models with IFTs of 5, 25 and 50 mN/m

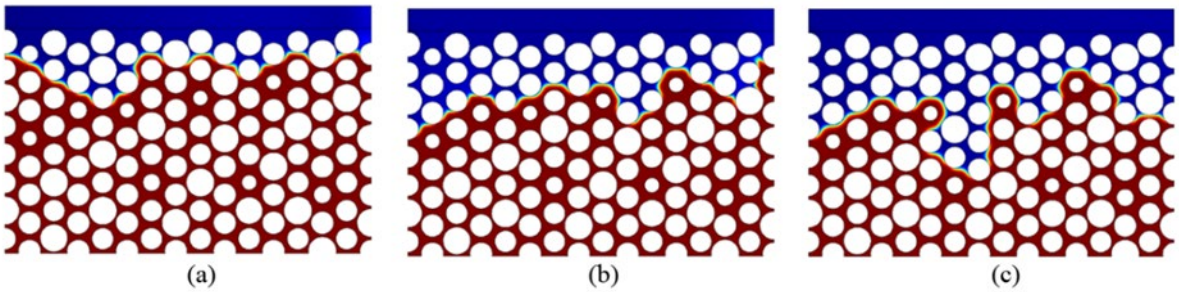

Figure 11. Snapshots of the stabilized fluid distributions for three models with (a)$\sigma = 5\frac{mN}{m}$, (b) $\sigma = 25\frac{mN}{m}$and (c) $\sigma = 50\frac{mN}{m}$

In the model with the lowest IFT, water phase progressed in a zone on the medium left hand side with the sizes of 2-3 pore bodies. In the rest of the medium, water phase has invaded upper grains with the size of 1-2 pore bodies (Figure 11a). As it is shown in Figure 11c, the model with the highest IFT has a progressed capillary finger in the middle of porous medium due to the higher capillary pressure. Figure 12 indicates the variation of the position of interface/ wall contact point with time for model of 50 mN/m IFT. The water surface slightly

oscillates during the filling fracture regime as a result of instantaneous start. Periodically oscillations of the water surface indicate contact angle variation during the process. The interface/ wall contact point exhibits an ascending behavior before the water front meets the outlet.

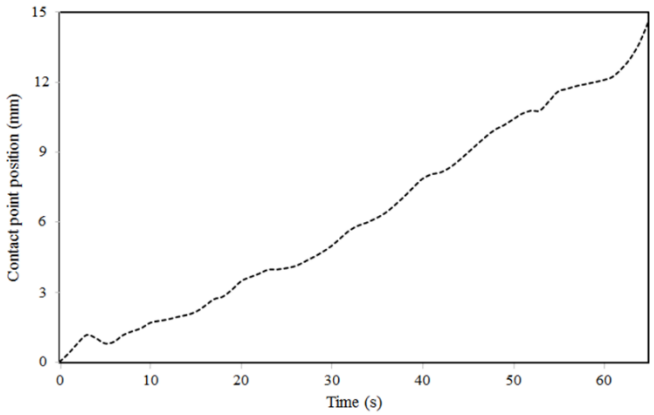

Figure 12. Position of the interface/wall contact point as a function of time for the model with IFT of 50 mN/m

3.4. Impact of water injection velocity

Figure 13 shows the recovery of matrix oil versus dimensionless time during the process of imbibition for water injection velocities of 0.05, 0.5 (the base case), and 5 mm/s. As it is observed, the model with the highest injection velocity of u_{inj}=5 mm/s, has recovered the matrix oil by 14% in the first 5 s and then rapidly reaches to its ultimate recovery. At injection velocity of 5 mm/s, water just invaded the fracture and the closest grains to the fracture and breakthrough occurred early (at t = 5 s) (See Figure 13). After stabilization, the model with injection velocity of 0.5 mm/s recovered almost 27% of the matrix oil. In the case of the model with the lowest injection velocity, the lowest imbibition rate and the highest ultimate recovery, i.e., 65%, can be observed. The matrix-fracture interactions are improved because the process takes place much slower compared to the other cases. The forces of viscous type causing fluids flow in the fracture, are not significant at this condition; thus, water could penetrate into most parts of the matrix. It was observed that water moves unstably forward and backward in the fracture. Water reached the outlet through the matrix and the fracture has not been occupied; thus, a later water breakthrough was observed (at t = 585 s). According to Figure 13, it can be concluded that at low injection rates, more time is needed to reach higher recovery.

As shown in Figure 14c, five oil blobs are trapped around the smallest grains, due to the lower capillary pressures. Besides, the expelled oil formed a pistonlike plug in the fracture which blocked water flow through the fracture. As a result of this phenomenon, more water can imbibe into the matrix and thus larger amount of oil is expelled from the matrix into the fracture. Figure 14b shows that water phase has progressed into the porous matrix with three capillary fingers. In the case of the model with u_{inj}=5 mm/s, absence of blocking effect and existence of larger shear force prevent formation and growth of oil droplets which result in reduction in the imbibition rate. Figure 14a reveals that the water infiltration path is less selective compared to the other cases; consequently, the water front progresses almost uniformly downward. This regime is characterized as the "instantly filled fracture" which is in agreement with micro-model observations made by Rangel-German and Kovscek [20]. It can be found that by increasing water injection velocity, the oil recovery factor and the imbibition depth decrease. Figure 15a illustrates that the movement of water-oil contact line happens on the marked grain surface until the water phase takes the whole grain. This figure also shows that the oil phase film between the grains narrows as the water phase bridges between the adjacent pores and the interface coalescence occurs. Figure 15b shows that the reverse displacement at the pore-level as a consequence of pressure gradient decreases across the fracture.

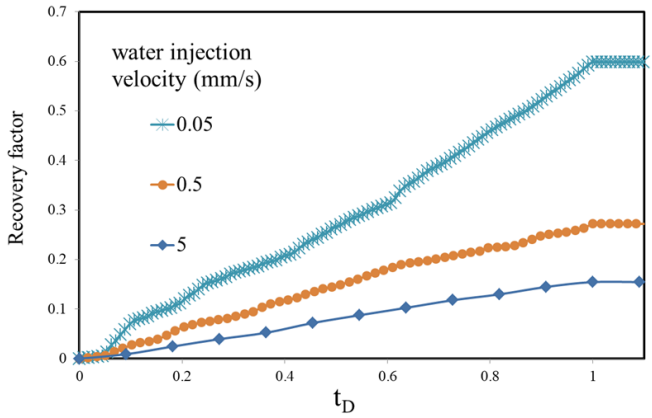

Figure 13. The matrix oil recovery factor as a function of dimensionless time for three models with different water injection velocities of 0.05, 0.5, and 5 mm/s

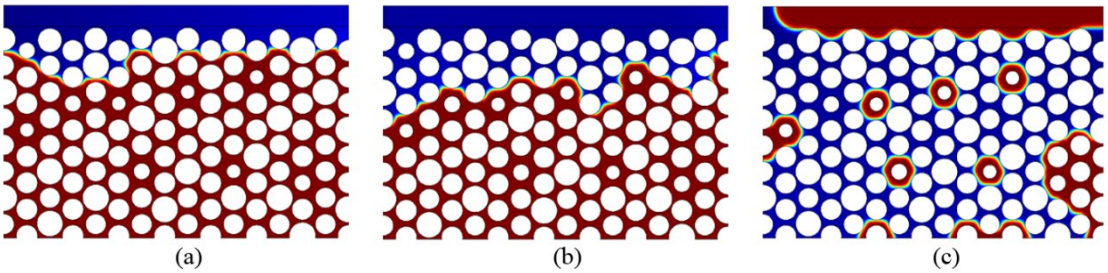

Figure 14. Snapshots of the stabilized fluid distributions for three models with different water injection velocities (a) u_{inj}=5, (b) u_{inj}=0.5, and (c) u_{inj}=0.05 mm/s

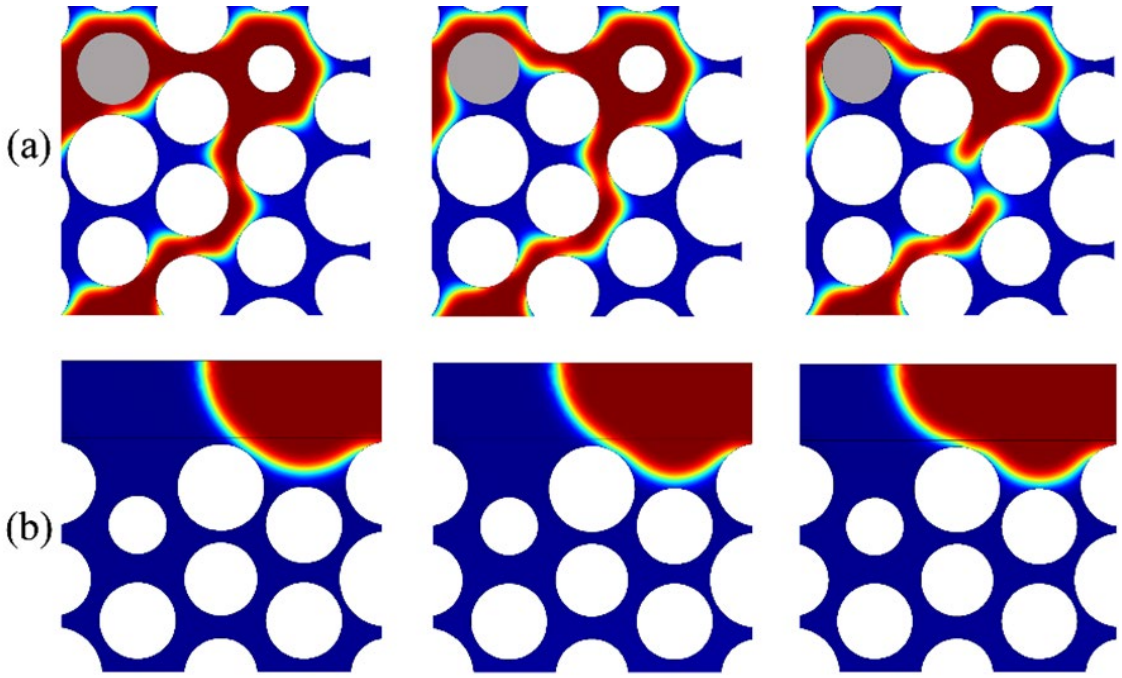

Figure 15. An enlarged section of the simulated model with u_{inj}=0.05 mm/s at three successive instants during the imbibition process

4. Conclusions

A precise-pore-scale model using the phase-field method was provided to investigate the matrix-fracture interaction during capillary imbibition. An accurate finite element solver was applied to solve the coupled Navier–Stokes and Cahn–Hilliard phase-field equations. A 2D heterogeneous matrix block and an adjacent fracture were established to be considered as computational domain. The constructed domain was discretized into triangular elements and the governing equations were solved in 2D space. Both matrix block and fracture were initially saturated with oil phase and the constant velocity water was injected at the fracture inlet to maintain continuous water supply and expel the oil phase. Different sensitivity analyses were implemented to study the effects of wettability, fracture aperture, IFT, and water injection velocity on the process of displacement. For the models with $\theta > \frac{\pi}{6}$, water just progressed in the fracture and could not propagate into the matrix block. While, for the strongly water-wet mediums $\left(\theta \frac{\leq \pi}{6}\right)$, water invaded more pore bodies and capillary fingers propagated into the matrix. It was found that decreasing the contact angle has a considerable impact on imbibition rate and ultimate oil recovery. It was also observed that the water mass imbibed into the matrix block varies linearly as a function of time before the water front meets the outlet, which was characterized as "filling fracture" regime. Higher imbibition rate and ultimate oil recovery could be reached by increasing the IFT. As an example, in the first 50 s, 16% of the matrix oil recovery was observed in the model with the lowest IFT ($\sigma = 5 \frac{mN}{m}$). While for the model with highest IFT ($\sigma = 50 \frac{mN}{m}$), ultimate oil recovery was higher than 30%. Increasing the fracture aperture decreased both water breakthrough time and oil recovery; however, the ultimate recovery was not significantly affected. The results revealed that 14% of matrix oil recovery observed in the first 5 s and rapidly reached to its ultimate recovery for the case with the highest injection velocity (u_{inj} =5 mm/s). While the lowest imbibition rate and the highest ultimate recovery (65%) were observed for the model with lowest injection velocity of (u_{inj} =0.05 mm/s). The model with u_{inj}=0.05 mm/s had capability to show some mechanisms at the pore-level such as oil trapping, reverse displacement, thinning of oil film, movement of fluids' contact line, interface coalescence, and bridging of water films. The constructed model could be applied as a benchmark for qualitative and quantitative study of the phenomenon and also for phase-field counter-current simulations.

References

[1] Gauteplass J, Follesø H, Graue A, Kovscek A, and Fernø M. Visualization of pore-level displacement mechanisms during CO_2 injection and EOR processes. Conference Proceedings, IOR 2013 - 17th European Symposium on Improved Oil Recovery, Apr 2013, cp-342-00024; ISBN: 978-90-73834-45-3.

[2] Park JW, Jiao K, and Li X. Numerical investigations on liquid water removal from the porous gas diffusion layer by reactant flow. Applied Energy, 2010; 87: 2180.

[3] Matthai SK, Mezentsev AA, Belayneh M. Finite element-node-centered finite-volume two-phase-flow experiments with fractured rock represented by unstructured hybrid-element meshes. SPE Reservoir Evaluation & Engineering, 2007; 10: 740-756.

[4] Juanes R, Spiteri E, Orr Jr F, & Blunt M. Impact of relative permeability hysteresis on geological CO2 storage. Water resources research, 2006; 42(12): W12418.

[5] Harrar WG, Murdoch LC, Nilsson B, Klint KES. Field characterization of vertical bromide transport in a fractured glacial till. Hydrogeology Journal, 2007; 15: 1473-1488.

[6] Zendehboudi S, Chatzis I, Shafiei A, Dusseault MB. Empirical modeling of gravity drainage in fractured porous media. Energy & Fuels, 2011; 25: 1229-1241.

[7] Simmons CT, Fenstemaker TR, Sharp Jr JM. Variable-density groundwater flow and solute transport in heterogeneous porous media: approaches, resolutions and future challenges. Journal of contaminant hydrology, 2001; 52: 245-275.

[8] Tanino Y, Zacarias-Hernandez X, Christensen M. Oil/water displacement in microfluidic packed beds under weakly water-wetting conditions: competition between precursor film flow and piston-like displacement. Experiments in Fluids, 2018; 59: 1-11.

[9] Amiri HA, Hamouda AA. Pore-scale modeling of non-isothermal two phase flow in 2D porous media: Influences of viscosity, capillarity, wettability and heterogeneity. International Journal of Multiphase Flow, 2014; 61: 14-27.
[10] Farzaneh S, Kharrat R, Ghazanfari M. Experimental study of solvent flooding to heavy oil in fractured five-spot micro-models: the role of fracture geometrical characteristics. Journal of Canadian Petroleum Technology, 2010; 49: 36-43.
[11] Maaref S, Rokhforouz MR, Ayatollahi S. Numerical investigation of two phase flow in micro-model porous media: Effects of wettability, heterogeneity, and viscosity. The Canadian Journal of Chemical Engineering, 2017; 95: 1213-1223.
[12] Zhang C, Oostrom M, Wietsma TW, Grate W, Warner M. G. Influence of viscous and capillary forces on immiscible fluid displacement: Pore-scale experimental study in a water-wet micromodel demonstrating viscous and capillary fingering. Energy & Fuels, 2011; 25: 3493-3505.
[13] Behbahani HS, di Donato G, Blunt MJ. Simulation of counter-current imbibition in water-wet fractured reservoirs. Journal of Petroleum Science and Engineering, 2006; 50: 21-39.
[14] Delijani EB, Pishvaie MR. Green Element solution of one-dimensional counter-current spontaneous imbibition in water wet porous media. Journal of Petroleum Science and Engineering, 2010; 70: 302-307.
[15] Standnes DC. Scaling group for spontaneous imbibition including gravity. Energy & fuels, 2010; 24: 2980-2984.
[16] Mirzaei-Paiaman A, Masihi M, Standnes DC. An analytic solution for the frontal flow period in 1D counter-current spontaneous imbibition into fractured porous media including gravity and wettability effects. Transport in porous media, 2011; 89: 49-62.
[17] Mirzaei-Paiaman A, Saboorian-Jooybari H. A method based on spontaneous imbibition for characterization of pore structure: Application in pre-SCAL sample selection and rock typing. Journal of Natural Gas Science and Engineering, 2016; 35: 814-825.
[18] Morrow NR, Mason G. Recovery of oil by spontaneous imbibition. Current Opinion in Colloid & Interface Science, 2001; 6: 321-337.
[19] Mason G, Morrow NR. Developments in spontaneous imbibition and possibilities for future work. Journal of Petroleum Science and Engineering, 2013; 110: 268-293.
[20] Rangel-German E, Kovscek AR. Experimental and analytical study of multidimensional imbibition in fractured porous media. J. of Petrol. Science and Engineering, 2002; 36**,** 45-60.
[21] Fernø M, Haugen Å, Graue A. Wettability effects on the matrix–fracture fluid transfer in fractured carbonate rocks. Journal of Petroleum Science and Engineering, 2011; 77: 146-153.
[22] Karadimitriou N, Hassanizadeh S. A review of micromodels and their use in two-phase flow studies. Vadose Zone Journal, 2012; 11: vzj2011. 0072.
[23] Rokhforouz M, Amiri HA. Pore-level influence of micro-fracture parameters on visco-capillary behavior of two-phase displacements in porous media. Advances in Water Resources, 2018; 113: 260-271.
[24] Rokhforouz MR, Amiri HA. Pore-level influence of wettability on counter-current spontaneous imbibition. 79th EAGE Conference and Exhibition 2017, 2017. European Association of Geoscientists & Engineers, 1-3.
[25] Hatiboglu CU, Babadagli T. Experimental and visual analysis of co-and counter-current spontaneous imbibition for different viscosity ratios, interfacial tensions, and wettabilities. Journal of Petroleum Science and Engineering, 2010; 70: 214-228.
[26] Rangel-German E, Kovscek AR. A micromodel investigation of two-phase matrix-fracture transfer mechanisms. Water resources research, 2006; 42(3): W03401.
[27] Hatiboglu CU, Babadagli T. 2008. Pore-scale studies of spontaneous imbibition into oil-saturated porous media. Physical Review E, 2008; 77: 066311.
[28] Raeini, AQ, Bijeljic B, Blunt MJ. Numerical modelling of sub-pore scale events in two-phase flow through porous media. Transport in porous media, 2014; 101: 191-213.
[29] Meakin P, Tartakovsky AM. Modeling and simulation of pore-scale multiphase fluid flow and reactive transport in fractured and porous media. Reviews of Geophysics, 2009; 47: RG3002.
[30] Zendehboudi S, Elkamel A, Chatzis I, Ahmadi MA, Bahadori A, Lohi A. Estimation of breakthrough time for water coning in fractured systems: Experimental study and connectionist modeling. AIChE Journal, 2014; 60: 1905-1919.
[31] Blunt MJ. Flow in porous media—pore-network models and multiphase flow. Current opinion in colloid & interface science, 2001; 6: 197-207.
[32] Raeini AQ, Bijeljic B, Blunt MJ. Generalized network modeling: Network extraction as a coarse-scale discretization of the void space of porous media. Phys. Review E, 2017; 96: 013312.

[33] Ahrenholz B, Tölke J, Lehmann P, Peters A, Kaestner A, Krafczyk M, Durner W. Prediction of capillary hysteresis in a porous material using lattice-Boltzmann methods and comparison to experimental data and a morphological pore network model. Advances in Water Resources, 2008; 31: 1151-1173.
[34] Porter ML, Schaap MG, Wildenschild D. Lattice-Boltzmann simulations of the capillary pressure–saturation–interfacial area relationship for porous media. Advances in Water Resources, 2009; 32: 1632-1640
[35] Amiri M, Zahedi G, Yunan MH. Water saturation estimation in tight shaly gas sandstones by application of Progressive Quasi-Static (PQS) algorithm–A case study. Journal of Natural Gas Science and Engineering, 2015; 22: 468-477.
[36] Prodanović M, Bryant SL. A level set method for determining critical curvatures for drainage and imbibition. Journal of colloid and interface science, 2006; 304: 442-458.
[37] Luo L, Zhang Q, Wang X-P, Cai X-C. A parallel finite element method for 3D two-phase moving contact line problems in complex domains. J. of Sci Computing, 2017; 72: 1119-1145.
[38] Fakhari A, Geier M, Bolster D. A simple phase-field model for interface tracking in three dimensions. Computers & Mathematics with Applications, 2019; 78: 1154-1165.
[39] Jafari I, Masihi M, Nasiri Zarandi M. Numerical simulation of counter-current spontaneous imbibition in water-wet fractured porous media: Influences of water injection velocity, fracture aperture, and grains geometry. Physics of Fluids, 2017; 29: 113305.
[40] Rokhforouz M, Amiri HA. Effects of grain size and shape distribution on pore-scale numerical simulation of two-phase flow in a heterogeneous porous medium. Advances in Water Resources, 2019; 124: 84-95.
[41] Sabooniha E, Rokhforouz M-R, Ayatollahi S. Pore-scale investigation of selective plugging mechanism in immiscible two-phase flow using phase-field method. Oil & Gas Science and Technology–Revue d'IFP Energies Nouvelles, 2019; 74: 78.
[42] Fakhari A, Geier M, Bolster D. A simple phase-field model for interface tracking in three dimensions. Computers & Mathematics with Applications, 2019; 78: 1154-1165.
[43] Huang H, Meakin P, Liu M. Computer simulation of two-phase immiscible fluid motion in unsaturated complex fractures using a volume of fluid method. Water resources research, 2005; 41(12): W12413.
[44] Gunde A, Babadagli T, Roy SS, Mitra SK. Pore-scale interfacial dynamics and oil–water relative permeabilities of capillary driven counter-current flow in fractured porous media. Journal of Petroleum Science and Engineering, 2013; 103: 106-114.
[45] Andersen P, Evje S, Kleppe H.A model for spontaneous imbibition as a mechanism for oil recovery in fractured reservoirs. Transport in porous media, 2014; 101**:** 299-331.
[46] Amiri HA, Hamouda AA. Evaluation of level set and phase field methods in modeling two phase flow with viscosity contrast through dual-permeability porous medium. International Journal of Multiphase Flow, 2013; 52: 22-34.
[47] Rokhforouz M-R, Amiri HAA. Phase-field simulation of counter-current spontaneous imbibition in a fractured heterogeneous porous medium. Physics of Fluids, 2017; 29: 062104.
[48] Gu Q, Zhu L, Zhang Y, Liu H. 2019. Pore-scale study of counter-current imbibition in strongly water-wet fractured porous media using lattice Boltzmann method. Physics of Fluids, 2019; 31: 086602.
[49] Rokhforouz M-R, Rabbani A, Ayatollahi S, Taghikhani V. Numerical analysis of heat conduction treated with highly conductive copper oxide nanoparticles in porous media. Special Topics & Reviews in Porous Media,2016; 7(2):149-160.
[50] Cahn JW, Hilliard JE. Free energy of a nonuniform system. I. Interfacial free energy. The Journal of chemical physics,1958; 28: 258-267.
[51] Multiphysics, C. 2011. Version 4.2. COMSOL. Inc., http://www.comsol.com.
[52] Badalassi VE, Ceniceros HD, Banerjee S. Computation of multiphase systems with phase field models. Journal of computational physics, 2003; 190: 371-397.
[53] Fichot F, Meekunnasombat P, Belloni J, Duval F, Garcia A, Quintard M. 2007. Two-phase flows in porous media: Prediction of pressure drops using a diffuse interface mathematical description. Nuclear engineering and design, 2007; 237: 1887-1898.
[54] Jacqmin D. Calculation of two-phase Navier–Stokes flows using phase-field modeling. Journal of computational physics, 1999; 155: 96-127.
[55] Yue P, Feng JJ, Liu C, Shen J. 2004. A diffuse-interface method for simulating two-phase flows of complex fluids. Journal of Fluid Mechanics, 2004; 515: 293-317.

[56] Babadagli T. Dynamics of capillary imbibition when surfactant, polymer, and hot water are used as aqueous phase for oil recovery. Journal of colloid and interface science, 2020; 246: 203-213.
[57] Brown C, Neustadter E. The wettability of oil/water/silica systems with reference to oil recovery. Journal of Canadian Petroleum Technology,1980; 19: 100-110.
[58] Maghz, A, Mohebbi A, Kharrat R, Ghazanfari MH. Pore-scale monitoring of wettability alteration by silica nanoparticles during polymer flooding to heavy oil in a five-spot glass micromodel. Transport in porous media, 2011; 87: 653-664.
[59] Lenormand R, Touboul E, Zarcone C. Numerical models and experiments on immiscible displacements in porous media. Journal of fluid mechanics, 1988; 189: 165-187.
[60] Rezaveisi M, Ayatollahi S, Rostami B. 2012. Experimental investigation of matrix wettability effects on water imbibition in fractured artificial porous media. Journal of Petroleum Science and Engineering, 2012; 86: 165-171.

To whom correspondence should be addressed: professor Amir H. Mohammadi, Discipline of Chemical Engineering, School of Engineering, University of KwaZulu-Natal, Howard College Campus, King George V Avenue, Durban 4041, South Africa, E-mail: amir_h_mohammadi@yahoo.com